Nuclear Inst. and Methods in Physics Research, A 1014 (2021) 165732

Contents lists available at ScienceDirect

Nuclear Inst. and Methods in Physics Research, A

journal homepage: www.elsevier.com/locate/nima

EcoMug: An Efficient COsmic MUon Generator for cosmic-ray muon applications

D. Pagano [a,b,*], G. Bonomi [a,b], A. Donzella [a,b], A. Zenoni [a,b], G. Zumerle [c,d], N. Zurlo [e,b]

[a] Department of Mechanical and Industrial Engineering, University of Brescia, Italy
[b] Istituto Nazionale di Fisica Nucleare (INFN), Pavia, Italy
[c] Department of Physics and Astronomy, University of Padova, Padova, Italy
[d] Istituto Nazionale di Fisica Nucleare (INFN), Padova, Italy
[e] Department of Civil, Environmental, Architectural Engineering and Mathematics, University of Brescia, Italy

ARTICLE INFO

Keywords:
Cosmic muon generator
Muon tomography
Muon radiography

ABSTRACT

Applications of cosmic-ray (CR) muons have grown in numbers in the last decade. Measurements of flux attenuation (radiography) and scattering angles (tomography) of CR muons have been successfully applied to the inspection or monitoring of large natural and civil structures, to the search for heavy metals in container and trucks, to the control of nuclear wastes, and much more. In the present work, a new Monte Carlo generator of CR muons, called EcoMug and specifically designed for muon radiography and tomography applications, is presented. It is a header-only C++11 library, based on a parametrization of experimental data. Unlike other tools, EcoMug gives the possibility of generating from different surfaces (plane, cylinder and half-sphere), while keeping the correct angular and momentum distribution of generated tracks. For example, this flexibility allows for a very efficient generation of nearly horizontal muons, of great interest in many muon radiography and tomography applications, by using cylindrical or half-spherical generation surfaces. Finally, EcoMug also allows the generation of CR muons according to user-defined parametrizations of their differential flux. Main features of EcoMug, its mathematical foundation, as well as applications to selected study cases are presented.

1. Introduction

Our planet is continuously hit by particles, generally called *primary cosmic rays*, originating from several astrophysical sources. Approximately 85% of them are protons, 12% are α-particles, whereas heavier elements only represent a fraction of 3%. As the column density of the atmosphere is ~1000 g/cm^2 and the nuclear interaction length in air is ~90.0 g/cm^2, not a single primary cosmic ray arrives at the sea level [1]. Instead, usually at altitudes between 15 and 20 km, they interact with atomic nuclei of the air, initiating electromagnetic and/or hadronic cascades. Some of the particles produced in these processes, usually referred to as *secondary cosmic rays*, can survive enough to reach the Earth's surface.

At sea level, approximately 80% of all charged particles hitting the ground are *muons*, referred to as *cosmic-ray muons* (CR muons) in the following, and their flux, through a horizontal surface, is roughly equal to one particle per square centimeter and minute. The flux, however, largely changes with the momentum and zenith angle θ of the muons. The momentum spectrum is almost flat below 1 GeV/c, whereas starts decreasing between 1 GeV/c and 10 GeV/c. In the 10–100 GeV/c range this reduction steepens, reflecting the spectrum of the pions they are originated from, and steepens even further at higher momenta as very energetic pions tend to interact with the atmosphere before decaying [2]. The dependency on θ is, instead, due to the increased muon decay probability and the stronger absorption in the atmosphere for inclined directions and it is usually approximated as $I(\theta) = I(\theta = 0) \cdot \cos^2\theta$. Both flux dependencies on θ and momentum are clearly visible from the experimental data in Fig. 1, which shows the differential flux of the charged component of cosmic rays as a function of the momentum, for eight intervals of θ, as measured by the ADAMO detector [3]. This differential flux basically coincides with the muon flux, already from momenta of very few GeV/c. The knees at low momenta and large values of θ, in Fig. 1, are due to the electron component of measured cosmic rays.

Distributions of momentum and zenith angle are not independent. For large zenith angles, the parent pion of the muon travels for longer distances and, at higher altitudes (low density), the decay probability is increased with respect to the interaction probability. As a result, pions with inclined directions tend to produce higher energy muons in their decay.

As primary cosmic rays are positively charged, it is no surprise that an excess of positively charged muons over negative muons is observed.

* Corresponding author at: Department of Mechanical and Industrial Engineering, University of Brescia, Italy.
E-mail address: davide.pagano@unibs.it (D. Pagano).

https://doi.org/10.1016/j.nima.2021.165732
Received 22 June 2021; Received in revised form 4 August 2021; Accepted 9 August 2021
Available online 19 August 2021

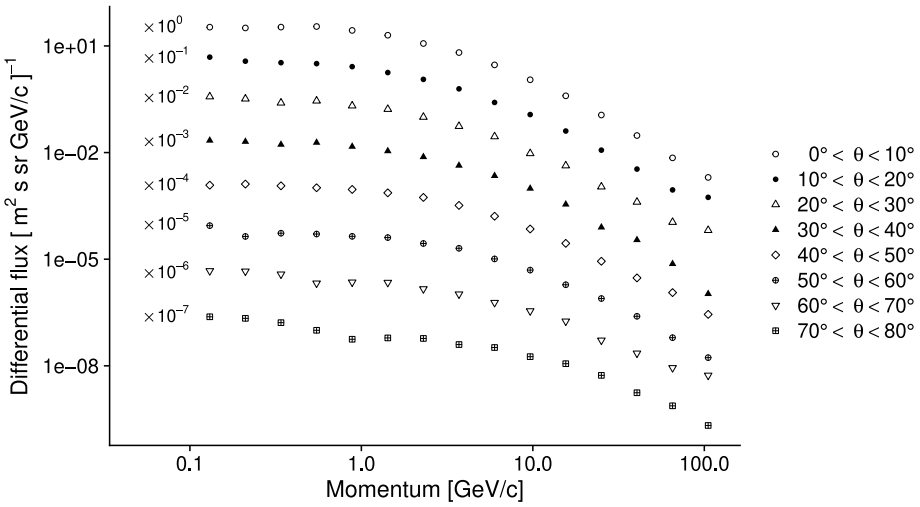

Fig. 1. Differential flux as a function of the momentum for eight intervals of the zenith angle θ, as measured by the ADAMO detector [3]. Measurements for each zenith angle interval have been multiplied by the factor reported on left to avoid overlaps.

The ratio $N(\mu^+)/N(\mu^-)$, called *charge ratio of muons*, is experimentally found to be constant over a wide momentum range and its value (at sea level) is ∼1.28 [2].

1.1. Application of cosmic-ray muons

Even though cosmic rays were discovered at the beginning of the 20th century, thanks to the studies of Pacini, Hess and others on the electric conductivity of air [4,5], it was only in the mid-1950s that they started to be used beyond the research domain only. In 1955, E.P. George estimated the thickness of rock above an underground tunnel, by measuring the flux attenuation of CR muons [6]. Similarly, the Nobel prize winner Luis W. Alvarez investigated the interior of the Chephren's pyramid at Giza, in search for possible new and unknown chambers in the stonework [7], finding no evidence of their existence. Both these applications were based on attenuation measurements of the CR muon flux, technique called *muon radiography*.

More recently, in 2003, scientists at Los Alamos National Laboratory proposed to use the scattering angle of CR muons, crossing a structure under investigation, to assess the properties of the crossed material [8]. This technique, called *muon tomography*, allows a three-dimensional image of the volume under investigation, at the cost of requiring the reconstruction of both the incoming and outgoing trajectories of CR muons. Since its proposal, muon tomography has been applied to the search for heavy metals for nuclear contraband detection [9], the search of shielded radioactive sources in scrap metal [10], the inspection of dry storage casks for spent nuclear fuel [11], the stability monitoring of civil structures [12] and much more.

Nowadays, all applications of muon radiography and tomography rely on simulation tools for the generation of the CR muons and their tracking through the system under study. While, in many cases, the choice of the tracking toolkit is reduced to only very few options, like GEANT4 [13] and FLUKA [14], for the generation of CR muons, instead, there is not such an agreement on the tools to be used. Many research groups use custom-made software, based on specific parametrizations and approximations of the flux of CR muons, whereas others rely on dedicated packages like CORSIKA [15] and CRY [16].

Muon radiography applications are sensitive to the angular distribution of CR muons, and many applications of muon tomography are also sensitive to their momentum distribution. For these reasons, an accurate simulation of the dependency of the muon flux on momentum and direction is a key requirement for every generation tool targeting to such applications. Moreover, as the inspection of large structures requires a very large statistics, the generator has also to be fast, preventing the use of accurate tools like CORSIKA [15], which simulate the full cascade of secondary particles initiated by primary cosmic rays.

In the present work a new Monte Carlo generator of CR muons, called EcoMug and specifically designed for muon radiography and tomography applications, is presented. It is a header-only C++11 library, which is based on a parametrization of data in Fig. 1. Unlike other tools, EcoMug gives the possibility of generation from different surfaces (plane, cylinder and half-sphere), while keeping the correct angular and momentum distribution of generated tracks. This flexibility allows, for example, for the very efficient generation of nearly horizontal muons, of great interest in many muon radiography and tomography applications, by using a cylindrical generation surface. In this way, there is no waste of CPU time in generating nearly vertical tracks, which are dominant in rate but of no interest to the specific application.

In the next section a non-comprehensive overview of the available tools for the generation of CR muons is given.

2. Cosmic-rays muons generators

Even though many applications in muon radiography and tomography rely on custom-made codes for the generation of CR muons, several tools for this task are currently available. Among them, we can perform the following coarse classification:

- *cosmic-ray air shower (CRAS) generators* - simulating the full cascade of secondary particles initiated by primary cosmic rays;
- *parametric generators* - using a parametrization of the flux of CR muons, based either on experimental data or on the results from simulations with CRAS generators;
- *special generators* - specifically designed for underground, high altitude or underwater experiments.

The previous classification is discussed in the following.

2.1. Cosmic-ray air shower generators

Accurate simulations of air showers are of paramount importance for many studies involving cosmic rays. For example, ultra high-energy primary cosmic rays, with energies of 10^{15} eV and above, can only be studied through the extensive air showers (EAS) they initiate in the atmosphere. For this reason, cosmic-ray air shower generators are used by experiments like IceCube [17], LOFAR [18], MAGIC [19], H.E.S.S. [20] and the Pierre Auger Observatory [21] to name a few.

The most popular CRAS generator, specifically tailored to the simulation of air showers initiated by primary cosmic rays, is CORSIKA, which is briefly described in the following.

CORSIKA [15] – CORSIKA (COsmic Ray SImulation for KAscade) is a Monte Carlo toolkit to simulate the evolution of EAS in the atmosphere initiated by photons, protons, nuclei or any other particle. All particles are tracked through the atmosphere until they either interact, decay or are absorbed. The hadronic interactions can be described by several reaction models, like EPOS-LHC, SIBYLL and QGSJET-II for high energies, and GHEISHA and UrQMD for lower energies. For the electromagnetic interactions, the user can choose between the shower program EGS4 [22] or the analytical NKG formulas [23]. Originally released in 1989, as a part of the detector simulation for the KASCADE experiment (as the name itself recalls), it has enormously evolved over the last three decades and, nowadays, it is used by almost all cosmic-ray, gamma-ray, and neutrino astronomy experiments [24]. At present CORSIKA is written in FORTRAN 77, which not only is no longer the main programming language in high energy or astroparticle physics, but suffers from limitations, like the memory management or the lack of object orientation. For these reasons, a complete rewriting of the code is in progress. Version 8 of the code, indeed, is based on modern C++ and Python [25].

The full simulation of the evolution of EAS is, of course, CPU intensive, making, in some cases, the use of CORSIKA unappealing. For this reason, tools like MCEq and CRY, described below, have been developed.

MCEq [26] – MCEq is a tool which numerically solves the equations describing the evolution of particle densities when propagating in a medium: this includes particle cascades in the Earth's atmosphere. The user can choose from different hadronic interaction models, parametrizations of primary cosmic-ray flux and density models for the atmosphere. MCEq provides the results in terms of differential energy spectra or total particle numbers.

CRY [16] – CRY is a generator of air showers induced by primary cosmic rays. The main difference with respect to CORSIKA is that here the simulation is based on precomputed input tables, produced by means of full MCNPX [27] simulations of protons, in the energy range of 1 GeV–100 TeV, injected at the top of the atmosphere. CRY still provides all produced particles (not only muons), reason why it has been included in the CRAS generators category, but at a fraction of the time required by CORSIKA. The user can choose to generate particle shower distributions at three different elevations (sea level, 2100 m and 11300 m) and has control over the geomagnetic cutoff and solar cycle effects. Of course, the gain in performance over CORSIKA comes at a cost in the form of some additional approximations: only protons for cosmic primaries, limited energy range, and simplified modeling of the atmosphere.

2.2. Parametric generators

For muon radiography and tomography applications, only CR muons are relevant, as they are the only particles which are penetrating enough to cross the structure of interest. Therefore, the generation and tracking of the cascade of secondary particles initiated by primary cosmic rays is totally unnecessary, especially considering the high statistics typically required by this kind of applications. In these cases, the most popular approach is to use parametric generators, where CR muons are generated according to a parametrization of their differential flux, based either on experimental data or on results from simulations with CRAS generators. Moreover, for parametric generators, it is possible to filter CR muons according to their momentum or direction before even generating them. This is particularly relevant, for example, for applications where large volumes are inspected, for which only muons with momentum above a certain threshold can cross the structure of interest.

There are very few general purpose software of this type as, very often, applications in muon radiography and tomography end up using custom made codes. An interesting exception is represented by the cosmic muon generator embedded in GEMC [28], which is a C++ framework that uses GEANT4 to simulate the passage of particles through matter. The generator is based on Dar's parametrization of the flux of atmospheric muons [29].

As an example of another possible approach to the design of a parametric generator, the CMSCGEN package is described in the following.

CMSCGEN [30] – The cosmic muon generator CMSCGEN has been designed for the CMS experiment, and is based on a parametrization of the differential muon flux at ground level, as obtained from simulations of the air showers with CORSIKA. From high-statistics samples of showers, initiated by protons with energies from 5 GeV to 10^7 GeV, the flux of muons, as a function of the momentum and for different values of the zenith angle, was fitted with polynomial functions. The polynomial approximation was found to be in good agreement not only with CORSIKA simulation data (in the range from 3 GeV to 3000 GeV) but also with experimental data from the L3 experiment [31].

2.3. Special generators

For some specific scenarios, like underground and underwater/ice experiments, dedicated tools for the generation of cosmic-ray muons have been developed. In the following, two notable examples are described.

muTeV [32] – muTeV is a FLUKA-based generator for TeV muons, mainly dedicated to the physics of high energy muons in underground or underwater experiments. The code, together with FLUKA, takes care of the interaction of primary cosmic ray in the atmosphere, modeled as a set concentric spherical shells, the air shower development, the transportation through the overburden (rock or sea), and the muon detection simulation. 3D profiles of the Gran Sasso mountain, as well as of the sea above two locations of underwater experiments, are already encoded in the software and new ones can be defined by the user.

Also for generators specifically designed for underground and underwater/ice experiments a parametric approach, as shown by MUPAGE, is possible.

MUPAGE [33] – MUPAGE has been developed to generate single and multiple atmospheric muon events, mainly for underwater/ice neutrino telescopes. MUPAGE relies on parametric formulas describing flux, angular distribution and energy of muon bundles, for water equivalent (w.e.) depths between 1.5 km to 5 km and zenith angles between 0 and 85°. The parametrization was obtained by means of MC simulations of primary cosmic ray interactions and shower propagation in the atmosphere, using the HEMAS code [34]. The choice of HEMAS (instead of the much more popular CORSIKA) was due to the fact that it was previously cross-checked with data from the underground MACRO experiment [35], operating from 1994 to 2000 at the Gran Sasso laboratories, at a w.e. depth comparable to that of neutrino telescopes.

3. Parametrization of the flux of cosmic-ray muons for EcoMug

EcoMug is a parametric generator, where the flux of CR muons at Earth's surface is modeled from the experimental data in Fig. 1. The parametrization of the experimental data and its use in EcoMug is presented in the following.

With reference to the coordinate system in Fig. 2, let $J(t, p, \theta, \phi)$ be the differential flux of CR muons at the Earth's surface, that is:

$$J \equiv J(t, p, \theta, \phi) = \frac{dN}{dt \cdot dp \cdot d\Omega \cdot dS_n}, \tag{1}$$

where dN is the number of particles, with momentum between p and $p + dp$, crossing a surface element dS_n orthogonal to the motion direction (θ, ϕ), within the solid angle $d\Omega$ and in the time dt. θ and ϕ are respectively the zenith and azimuthal angles of the muon direction, so the solid angle is $d\Omega = \sin\theta \; d\theta d\phi$.

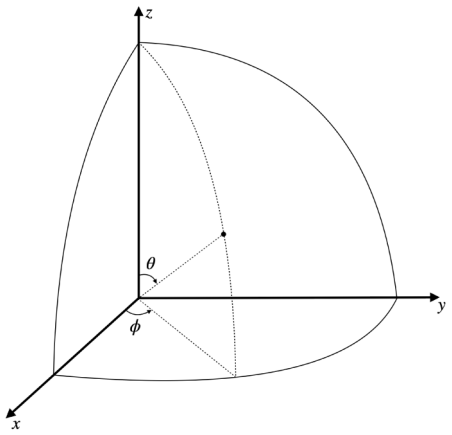

Fig. 2. Definition of the coordinate system used in EcoMug.

The experimental differential flux of CR muons, as measured in [3], can be parametrized by the following function [36]:

$$J = \left[1600 \cdot \left(\frac{p}{p_0} + 2.68\right)^{-3.175} \cdot \left(\frac{p}{p_0}\right)^{0.279}\right] \cdot (\cos\theta)^n \cdot \frac{1}{\mathrm{m}^2 \cdot \mathrm{s} \cdot \mathrm{sr} \cdot \mathrm{GeV/c}}, \tag{2}$$

where $p_0 = 1$ GeV/c and n is a function of p equal to

$$n(p) = \max\left[0.1,\ 2.856 - 0.655 \cdot \ln\left(\frac{p}{p_0}\right)\right],$$

with $p > 0.040$ GeV/c.

The comparison between experimental data and predictions from Eq. (2) is shown in Fig. 3. Markers represent the experimental differential flux as a function of the momentum and for eight zenith angle intervals, whereas the superimposed curves are the predictions from Eq. (2). As already mentioned in Section 1, experimental data measured the differential flux of the charged component in cosmic rays: while this basically coincides with the muon flux from already very few GeV/c, at lower momenta and large values of θ the contribution due to electrons is relevant. Because of this, measured flux starts to increase quickly as the momentum decreases. Chosen parametrization, however, does not include this effect, as only the muon component is relevant to EcoMug, resulting in a discrepancy for low momenta and large zenith angles.

In general, a parametric CR muon generator has to define the point of origin, direction and momentum of each muon, according to the corresponding probability density functions (which might not be independent). The way this generation is performed can be tailored to the geometry of the problem which is dealt with. In EcoMug, the origin points of generated muons can be sampled from a plane surface (*flat sky generation*), from a cylindrical surface or from a half-spherical surface, while keeping the correct angular and momentum distributions. The choice of one or another method should be based on the symmetry and geometrical features of the problem in study. In the following, a description of these three possible generation methods, which are available in EcoMug, is provided.

3.1. Flat sky generation

In many scenarios, it could be convenient to generate muons from a horizontal plane surface, to be placed on top of the system to be investigated. In analogy to Eq. (1), the differential flux of CR muons crossing an element of horizontal surface dS_z can be written as

$$J_z \equiv J_z(t, p, \theta, \phi) = \frac{dN}{dt \cdot dp \cdot d\Omega \cdot dS_z}. \tag{3}$$

By denoting with dS_n the projection of dS_z on a plane perpendicular to the muon direction, whose zenith angle is θ, Eq. (3) becomes

$$\begin{aligned} J_z &= \frac{dN}{dt \cdot dp \cdot d\Omega \cdot dS_n} \cdot \cos\theta \\ &= J \cdot \cos\theta \\ &= \left[1600 \cdot \left(\frac{p}{p_0} + 2.68\right)^{-3.175} \cdot \left(\frac{p}{p_0}\right)^{0.279}\right] \\ &\quad \cdot (\cos\theta)^{n+1} \cdot \frac{1}{\mathrm{m}^2 \cdot \mathrm{s} \cdot \mathrm{sr} \cdot \mathrm{GeV/c}}. \end{aligned} \tag{4}$$

Being $d\Omega = \sin\theta\ d\theta d\phi$, if we multiply Eq. (4) by $\sin\theta$, we obtain the number of particles, with momentum between p and $p+dp$, zenith angle between θ and $\theta+d\theta$, and azimuth angle between ϕ and $\phi+d\phi$, crossing a horizontal surface element dS_z in the time dt:

$$\begin{aligned} J'_z &\equiv \frac{dN}{dt \cdot dp \cdot d\theta \cdot d\phi \cdot dS_z} \\ &= \left[1600 \cdot \left(\frac{p}{p_0} + 2.68\right)^{-3.175} \cdot \left(\frac{p}{p_0}\right)^{0.279}\right] \\ &\quad \cdot (\cos\theta)^{n+1} \cdot \sin\theta \cdot \frac{1}{\mathrm{m}^2 \cdot \mathrm{s} \cdot \mathrm{sr} \cdot \mathrm{GeV/c}}. \end{aligned} \tag{5}$$

In the flat sky generation, the origin position of generated CR muons is uniformly distributed over the generation surface, the azimuth angle ϕ is uniform randomly generated in $[0, 2\pi]$ (or in a subset if requested by the user), and the momentum and zenith angle θ are sampled from the differential flux in Eq. (5). From a technical point of view, this sampling makes use of both the inverse transform sampling and acceptance–rejection methods [37], as J'_z is not invertible. Indeed, even though J'_z depends on p because of the product $[(p/p_0) + 2.68]^{-3.175} \cdot (p/p_0)^{0.279}$, the first factor is a much quicker changing function than the second one. Therefore, p is initially sampled from $(p+2.68)^{-3.175}$, using the inverse transform, and then the rejection acceptance–rejection method is applied to the remaining terms of J'_z: in this way the rejection rate of the method is significantly reduced. This strategy is also applied to the other generation methods.

3.2. Cylindrical generation

In other scenarios, as for example in muon scattering tomography of high structures like blast furnaces [38], it could be more convenient to generate muons from a cylindrical vertical surface, of finite height, surrounding the system of interest.

Let us consider a cylinder whose symmetry axis coincides with the z-axis of the reference frame in Fig. 2. Let dS_x be a surface element on the cylinder orthogonal to the x-axis and dS_n its projection on a plane perpendicular to the muon direction. Because of the symmetry in ϕ, for a cylindrical surface, we can choose the surface element orthogonal to the x-axis without loss of generality. By denoting with θ and ϕ the zenith and azimuthal angles of the muon direction, and with $\hat{x}$ and $\hat{n}$ the unit vectors orthogonal to dS_x and dS_n, dS_n can be written as

$$dS_n = dS_x\ \hat{x} \cdot \hat{n} = dS_x \sin\theta\cos\phi. \tag{6}$$

Using Eq. (6), the differential flux across a vertical surface becomes

$$\begin{aligned} J_x &\equiv \frac{dN}{dt \cdot dp \cdot d\Omega \cdot dS_x} \\ &= \frac{dN}{dt \cdot dp \cdot d\Omega \cdot dS_n} \cdot \sin\theta\cos\phi \\ &= \left[1600 \cdot \left(\frac{p}{p_0} + 2.68\right)^{-3.175} \cdot \left(\frac{p}{p_0}\right)^{0.279}\right] \\ &\quad \cdot (\cos\theta)^n \sin\theta\cos\phi \cdot \frac{1}{\mathrm{m}^2 \cdot \mathrm{s} \cdot \mathrm{sr} \cdot \mathrm{GeV/c}}. \end{aligned} \tag{7}$$

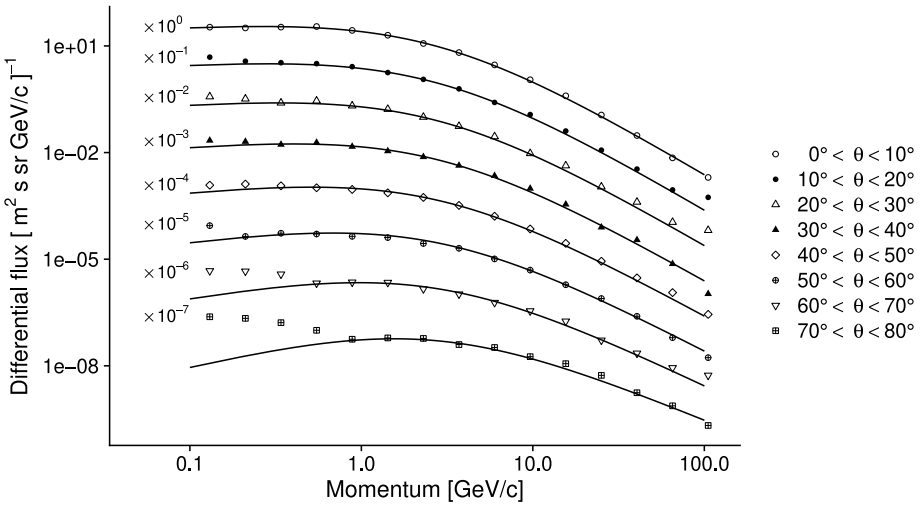

Fig. 3. Experimental differential flux, as a function of the momentum and for eight zenith angle intervals [3]. Superimposed curves are the predictions from Eq. (2) for the muon component only.

As for the flat sky generation, it is convenient to multiply J_x by $\sin\theta$ to define the J'_x differential flux:

$$J'_x \equiv \frac{dN}{dt \cdot dp \cdot d\theta \cdot d\phi \cdot dS_x} = \left[1600 \cdot \left(\frac{p}{p_0} + 2.68\right)^{-3.175} \cdot \left(\frac{p}{p_0}\right)^{0.279}\right] \cdot (\cos\theta)^n (\sin\theta)^2 \cos\phi \cdot \frac{1}{\mathrm{m}^2 \cdot \mathrm{s} \cdot \mathrm{sr} \cdot \mathrm{GeV/c}}. \tag{8}$$

The origin position of CR muons is uniform randomly chosen on the cylindrical generation surface, whereas the momentum, zenith angle θ and azimuth angle ϕ are sampled from the differential flux J'_x in Eq. (8). By noting that Eq. (8) only correlates p and θ, by means of the term n, we can independently generate ϕ, uniformly in $\cos\phi$, and then only sample the other two variables from J'_x, without the $\cos\phi$ term. In this way, the acceptance–rejection method is only applied to the momentum and zenith angle, as in the flat sky case, saving computation time.

3.3. Half-spherical generation

Always with reference to the coordinate system in Fig. 2, let us consider a half-sphere with the base laying on the x–y plane and centered with the origin. Let dS_t be a generic surface element on a half-sphere, orthogonal to the direction (θ_0, ϕ_0) and dS_n its projection on a plane perpendicular to the muon direction. In analogy to what is has been done for the cylindrical case, we can choose $\phi_0 = 0$ without loss of generality, because of the symmetry in ϕ of the half-sphere. By denoting with θ and ϕ the zenith and azimuthal angles of the muon direction, and with $\hat{t}$ and $\hat{n}$ the unit vectors orthogonal to dS_t and dS_n, dS_n can be written as

$$dS_n = dS_t\, \hat{t} \cdot \hat{n} = dS_t \left[\sin\theta_0 \sin\theta \cos\phi + \cos\theta_0 \cos\theta\right], \tag{9}$$

where *the law of cosines* was used. From Eq. (9), the differential flux across a generic surface element of a half-sphere becomes

$$J_t \equiv \frac{dN}{dt \cdot dp \cdot d\Omega \cdot dS_t} = \frac{dN}{dt \cdot dp \cdot d\Omega \cdot dS_n} \cdot \left[\sin\theta_0 \sin\theta \cos\phi + \cos\theta_0 \cos\theta\right] = \left[1600 \cdot \left(\frac{p}{p_0} + 2.68\right)^{-3.175} \cdot \left(\frac{p}{p_0}\right)^{0.279}\right] \cdot (\cos\theta)^n \left[\sin\theta_0 \sin\theta \cos\phi + \cos\theta_0 \cos\theta\right] \cdot \frac{1}{\mathrm{m}^2 \cdot \mathrm{s} \cdot \mathrm{sr} \cdot \mathrm{GeV/c}}. \tag{10}$$

As we did before, we can multiply J_t by $\sin\theta$ to define the J'_t differential flux:

$$J'_t \equiv \frac{dN}{dt \cdot dp \cdot d\theta \cdot d\phi \cdot dS_t} = \left[1600 \cdot \left(\frac{p}{p_0} + 2.68\right)^{-3.175} \cdot \left(\frac{p}{p_0}\right)^{0.279}\right] \cdot (\cos\theta)^n \left[\sin\theta_0 (\sin\theta)^2 \cos\phi + \cos\theta_0 \cos\theta \sin\theta\right] \cdot \frac{1}{\mathrm{m}^2 \cdot \mathrm{s} \cdot \mathrm{sr} \cdot \mathrm{GeV/c}}. \tag{11}$$

As expected, if $\theta_0 = 0$ Eq. (11) becomes equal to the one for the flat sky (Eq. (5)), whereas if $\theta_0 = \pi/2$ it becomes equal to the one for the cylindrical case (Eq. (8)).

Eq. (11) correlates not only p, θ and ϕ, but also θ_0, which, together with ϕ_0, defines the origin position of the CR muon on the half-sphere. For this reason, the sampling of all these variables from J'_t involves the use of the acceptance–rejection method in 4D space, resulting in a worsening of the generation speed with respect to the other methods, as discussed in the next sections.

4. Comparison between the different generation methods

The generation methods discussed above, and implemented in EcoMug, are mathematically equivalent, provided that all of them grant the proper coverage of the geometrical acceptance of the detection system. However, depending on the case study, one method could be more effective than the others, in respect to the generation time. In this section, a comparison of the performance of the three generation methods, for three different scenarios, is presented.

4.1. Vertical plane detectors

In muon tomography applications, scenarios where two (or more) vertical detectors are placed around the structure to be investigated are quite common. Muons are requested to be reconstructed by both detectors in order to measure their incoming and outcoming directions. In these cases, the generation of muons from a flat sky is extremely inefficient, as detected muons have large zenith angles. Fig. 4 schematizes this tomography-like scenario, referred to as configuration C1 in the following, where two plane detectors of area 125 cm × 250 cm are placed in front of each other at a distance of 300 cm. Performance of the cylindrical and half-spherical generations were compared and

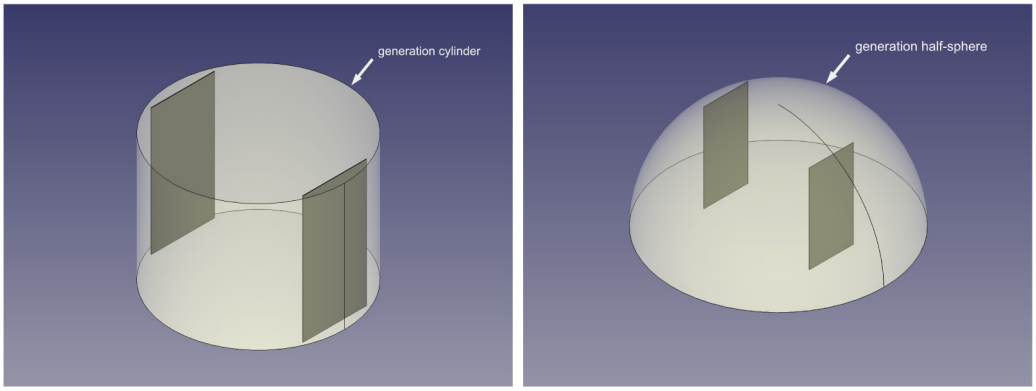

Fig. 4. Scheme of configuration C1 with the cylindrical (left) and the half-spherical (right) generation surfaces.

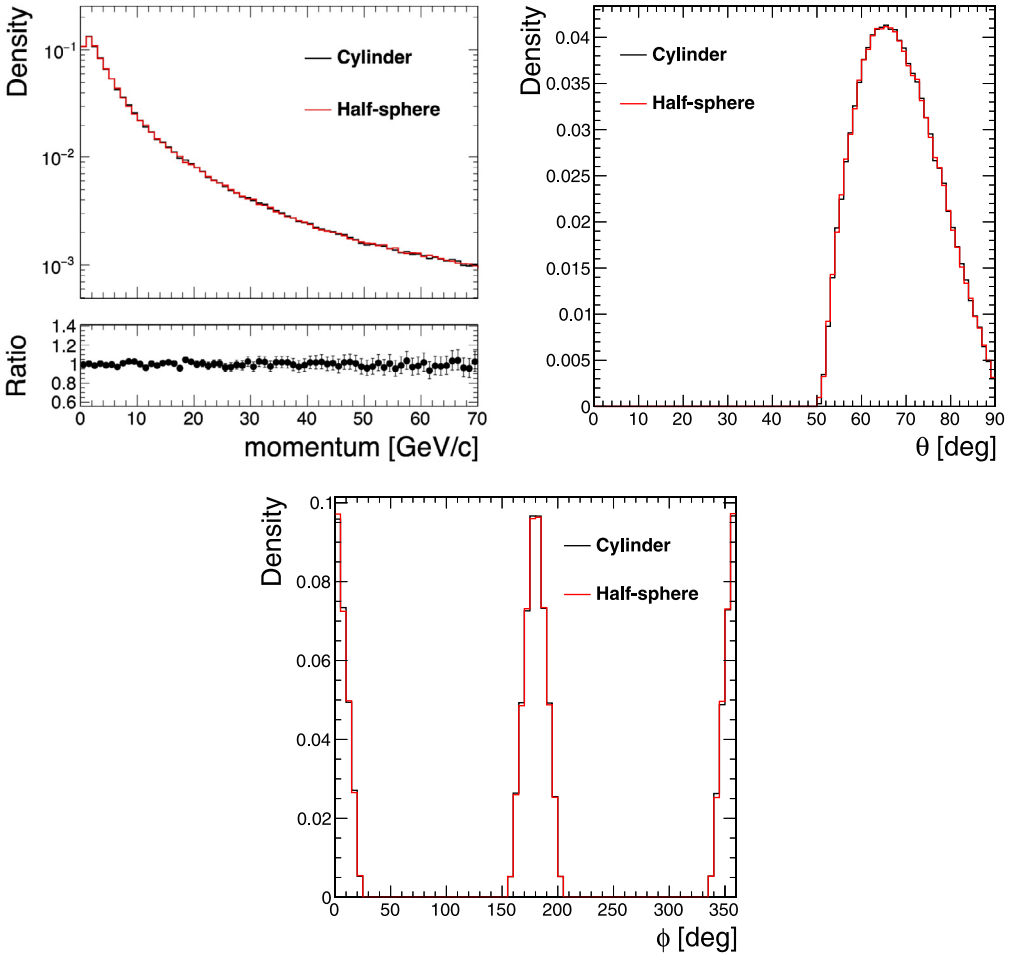

Fig. 5. Comparison between the momentum (top left), the zenith angle θ (top right) and azimuthal angle ϕ (bottom) for the detected muons in the configuration C1.

the results are shown in Fig. 5, where both generation surfaces were designed to grant the full coverage of the detection system.

As expected, the distributions for momentum, zenith angle, and azimuthal angle, for muons crossing both detectors, are equivalent. The plane generation was not included in this test, as only an infinite large surface would allow for muons with zenith angles up to $\theta = 90°$ to be detected. Even though the results from the cylindrical and the half-spherical generations are equivalent, the latter is approximately a factor 4 slower, because of the smaller generation efficiency, that is the ratio of the number of detected muons to the generated ones.

In a more realistic scenario, some of the authors have successfully used the generation from a cylindrical surface for muon tomography studies of a blast furnace [38].

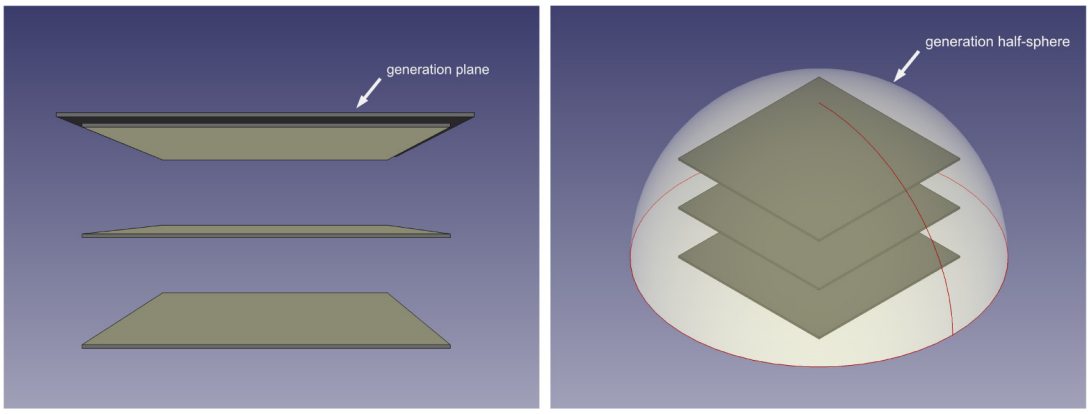

Fig. 6. Scheme of configuration C2 with the plane (left) and the half-spherical (right) generation surfaces.

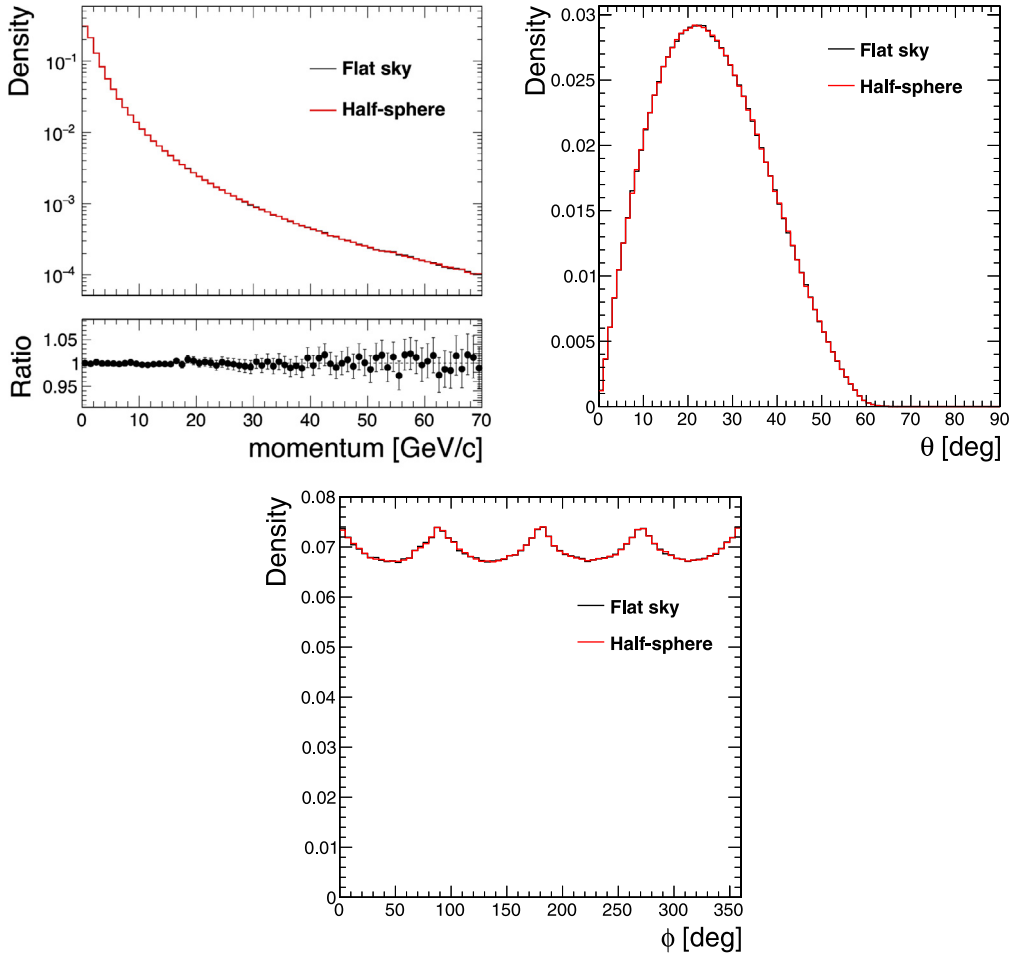

Fig. 7. Comparison between the momentum (top left), the zenith angle θ (top right) and azimuthal angle ϕ (bottom) for the detected muons in the configuration C2.

4.2. Horizontal plane detectors

Another common scenario is represented by muon telescopes, that is tracking detectors consisting of two or more sensitive layers, used to reconstruct the direction of the incoming muons. Figs. 6 schematize a muon telescope with three layers, of 100 cm × 100 cm area, placed at a vertical distance of 30 cm from each other. For this scenario, referred to as configuration C2 in the following, we considered the generation from a plane, slightly larger than the layers and placed very close to the topmost one, and from a half-sphere, whose radius was close to the smallest one to grant the full coverage of the detector. We did not consider the generation from a cylindrical surface, as it is not well suited to this setup.

Not only the distributions for momentum, zenith angle, and azimuthal angle, for muons crossing all the detectors, are equivalent as shown in Figs. 7, but we notice also in this case the performance-wise differences discussed for the configuration C1: the half-spherical generator took 11.6 s to generate 100k muons crossing all detectors,

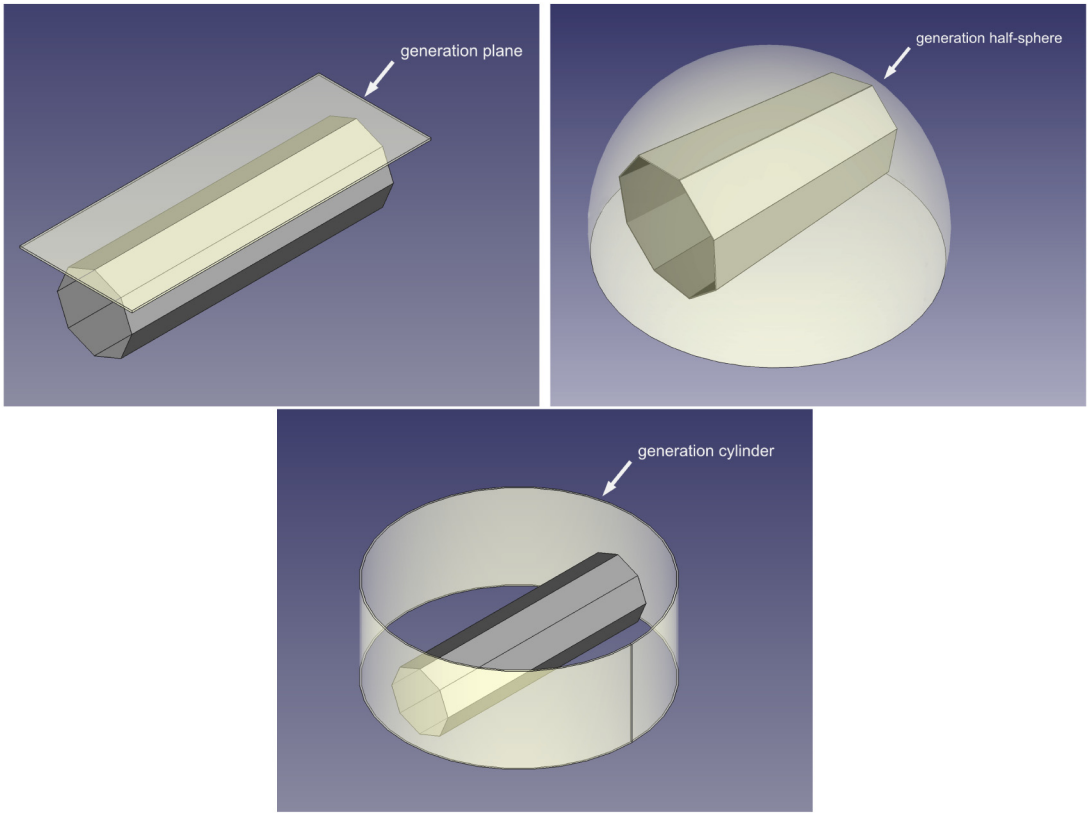

Fig. 8. Scheme of configuration C3 with the plane (top left), the half-spherical (top right) and the cylindrical (bottom) generation surfaces. Both plane and cylindrical surfaces are in their S sizes, as described in the text.

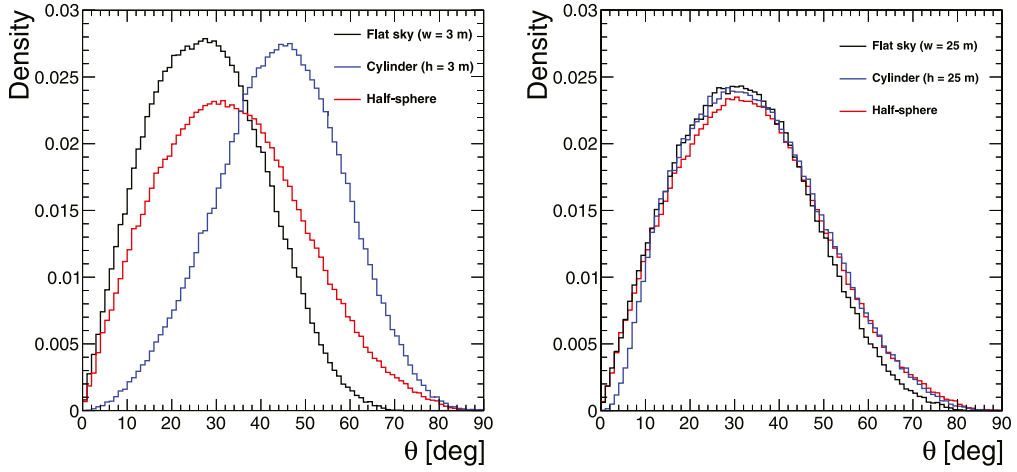

Fig. 9. Comparison between the zenith angle distributions for the detected muons in the configuration C3. The plot on the left (right) corresponds to plane and cylindrical surfaces in their S (L) sizes, as described in the text.

whereas the plane one only took 2.65 s (on a 2.6 GHz Intel Core i7 6 core).

4.3. Octagonal tracking detector

The last comparison involves a more complex detector, consisting of eight sensitive layers arranged in an octagonal configuration, inspired to inner tracking detectors of some experiments at colliders. The radius and length of the detector were chosen respectively equal to 1 m and 4 m. For this setup, referred to as configuration C3 in the following and shown in Fig. 8, all three generation methods were tested. For the half-sphere generation, the surface was chosen to be close to the smallest one to fully contain the detector, whereas for the plane and cylindrical generations two sizes were considered:

- S – corresponding to a plane surface of width $w = 3$ m and length $l = 5$ m, and to a cylindrical surface of height $h = 3$ m and radius $r = 2.5$ m, as shown in Figs. 8;
- L – corresponding to a plane surface of width $w = 25$ m and length $l = 5$ m, and to a cylindrical surface of height $h = 25$ m and radius $r = 2.5$ m.

The plane generation was placed close to the upmost layer of the detector and oriented as in Fig. 8 (top left). For both the plane and

cylindrical generations, the full coverage of the detector acceptance cannot be achieved in neither of the two sizes considered.

Figs. 9 show the zenith angle distributions, for generated muons crossing any two of the sensitive layers, for the three generations methods. The plot on the left refers to the S sizes and shows large discrepancies between the curves, as muons from both the plane and cylindrical surfaces are geometrically limited in θ, in the high and low region respectively. Because of the correlation between θ and ϕ of detected muons, introduced by the detector geometry, large discrepancies are also visible for the azimuthal angle distribution too, as shown in Fig. 10 (left).

As the size of these generation surfaces increases, though, the corresponding θ and ϕ distributions tend to the ones of the half-sphere, as shown in Figs. 9 (right) and 10 (right). Finally, since the differential flux, as modeled by Eq. (2), correlates p and θ, also the momentum distribution shows the same behavior, though to a lesser extent, as shown in Figs. 11.

With the increase of their sizes, though, plane and cylindrical generation surfaces become less efficient, as an increasing number of generated muons do not cross the detector. In the configuration with the L sizes, plane and cylindrical generation surfaces were respectively a factor 2.5 and 1.7 slower than the half-spherical case.

In a more realistic scenario, the half-spherical generation surface has been used by some of the authors for CR muons generation for the AEgIS experiment at CERN [39].

All previous case studies have shown that the three generation methods in EcoMug are equivalent, provided they all grant the full coverage of the detection system. Therefore, the choice of a method over another should be based on the geometrical features of the specific case study. In the next section an overview of the library EcoMug and its usage is given.

5. EcoMug Library

EcoMug is a C++11 library which implements the generation methods described in Section 3. It has been designed as a header-only library, that is the full definitions of classes and functions are exposed to the compiler by means of a single header file. This makes extremely easy to integrate EcoMug in any C++ project: it is enough to point the compiler at the location of the EcoMug.h file, and then `#include` the header files into the source of the project. The code is available at https://github.com/dr4kan/EcoMug under the GPL-3.0 license.

5.1. Basic usage

The use of the library requires the initialization of the `EcoMug` class, the choice of the generation method, and the definition of the size and position of the generation surface, as in the example codes 1, 2 and 3.

```
EcoMug gen; // initialization of the class
gen.SetUseSky(); // plane surface generation
gen.SetSkySize({{10., 10.}}); // x and y size of the plane
// (x,y,z) position of the center of the plane
gen.SetSkyCenterPosition({{0., 0., 20.}});
```

Example code 1: EcoMug setup for a flat surface generation.

```
EcoMug gen; // initialization of the class
gen.SetUseCylinder(); // cylindrical surface generation
gen.SetCylinderRadius(10.); // cylinder radius
gen.SetCylinderHeight(30.); // cylinder height
// (x,y,z) position of the center of the cylinder
gen.SetCylinderCenterPosition({{0., 0., 15.}});
```

Example code 2: EcoMug setup for a cylindrical surface generation.

```
EcoMug gen; // initialization of the class
gen.SetUseHSphere(); // half-spherical surface generation
gen.SetHSphereRadius(30.); // half-sphere radius
// (x,y,z) position of the center of the half-sphere
gen.SetHSphereCenterPosition({{0., 0., 0.}});
```

Example code 3: EcoMug setup for a half-spherical surface generation.

The reference frame used in EcoMug is shown Fig. 2. Once the setup of the instance of the `EcoMug` class is done, the generation of a cosmic-ray muon can be invoked with the method `Generate()`, which will compute its position, direction, momentum, and charge. All these quantities can be accessed with the methods `GetGenerationPosition()`, `GetGenerationTheta()`, `GetGenerationPhi()`, `GetGenerationMomentum()`, and `GetCharge()`, as shown in the example code 4. The charge for generated muons takes into account the excess of positive muons over negative ones, as described in Section 1, assuming a constant charge ratio. Angles are in radians, momentum is in GeV/c, whereas the unit of measure of the position is arbitrary and depends on the choice done in the simulation code where EcoMug is used. In Appendix an example of the integration with GEANT4 is provided.

```
// Setup of the instance of the EcoMug class
// as in the example code 1
EcoMug gen;
gen.SetUseSky();
gen.SetSkySize({{10., 10.}});
gen.SetSkyCenterPosition({{0., 0., 20.}});

// The array storing muon generation position
std::array<double, 3> muon_position;

// Loop to generate 1000 cosmic-ray muons
for (auto event = 0; event < 1000; ++event) {
  gen.Generate(); // generate a cosmic-ray muons

  // access position, direction and momentum
  // pleas note that GetGenerationPosition()
  // returns a std::array<double, 3>
  muon_position = gen.GetGenerationPosition();
  double muon_p = gen.GetGenerationMomentum();
  double muon_theta = gen.GetGenerationTheta();
  double muon_phi = gen.GetGenerationPhi();
  double muon_charge = gen.GetCharge();

  ... // the code where generated CR muons are used
}
```

Example code 4: Accessing position, direction, momentum and charge of generated cosmicray muons in EcoMug.

5.2. Seeding the generator

As already mentioned, the generation of a CR muon in EcoMug involves the use of the acceptance–rejection method in a 2D space, for a flat and cylindrical surface, and in a 4D space, for the half-spherical surface, to sample according to the distributions described in Section 3. For this reason a very fast and reliable pseudo-random number generator (PRNG) is necessary. EcoMug internally uses a class called `EMRandom`, which is based on the xoroshiro128+ algorithm [40], the fastest PRNG at the time of writing. The time required to generate 1M muons, using a compiled code with the `-O3` flag on a 2.6 GHz Intel Core i7 6 core, is on average:

- 1.3 s for the flat sky generator;
- 2.6 s for the cylindrical generator;

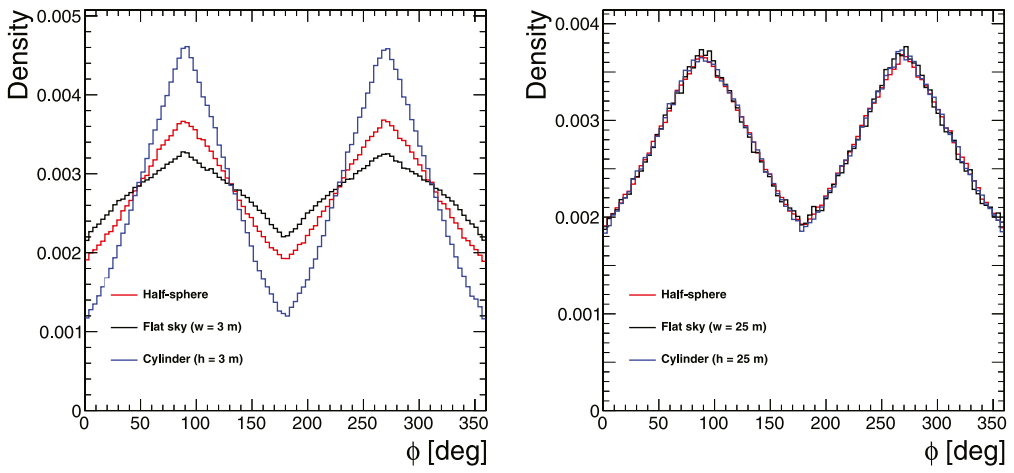

Fig. 10. Comparison between the azimuthal angle distributions for the detected muons in the configuration C3. The plot on the left (right) corresponds to plane and cylindrical surfaces in their S (L) sizes, as described in the text.

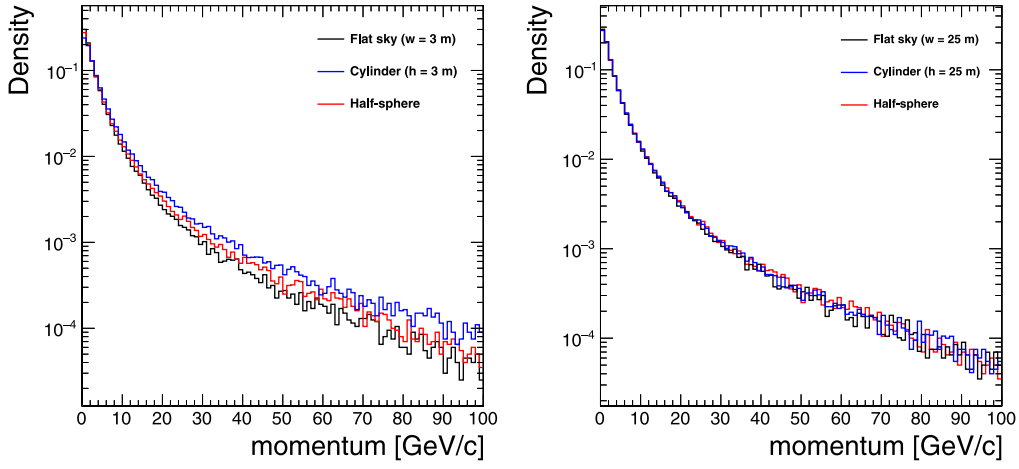

Fig. 11. Comparison between the momentum distributions for the detected muons in the configuration C3. The plot on the left (right) corresponds to plane and cylindrical surfaces in their S (L) sizes, as described in the text.

- 4.9 s for the half-sphere generator.

Previous numbers do not include any check on the angular variables or momentum of generated tracks, nor the time necessary for their tracking.

It is possible to set the seed in EcoMug, for reproducible generations. This can be done with the method `SetSeed`, as shown in the example code 5. If the seed is set to 0 (or the method is not invoked at all), a random seed is used.

```
EcoMug gen;
gen.SetUseSky();
gen.SetSkySize({{10., 10.}});
gen.SetSkyCenterPosition({{0., 0., 20.}});

// set the seed (only positive integers are accepted)
gen.SetSeed(1234);
```

Example code 5: Setting a seed in EcoMug.

5.3. Filtering cosmic-ray muons at generation level

Experimental data, used to model the cosmic-ray flux in Eq. (2), involve muons with momentum up to approximately 100 GeV/c and zenith angle up to 80°. However, as for many applications in muon radiography and tomography, high energy and nearly horizontal cosmic-ray muons are of utmost importance, by default EcoMug generates them with momentum up to 1000 GeV/c and zenith angles up to 90°. The user should keep in mind, though, that Eq. (2) could not describe accurately the flux outside the range of experimental data, even though this can be fixed by resorting to reweighting techniques.

In several scenarios, one could be interested in generating tracks from a subset of these parameters, saving space and computation time. EcoMug allows this by exposing to the user the following methods:

- `SetMinimumMomentum` - Set the minimum momentum for generated cosmic-ray muons;
- `SetMaximumMomentum` - Set the maximum momentum for generated cosmic-ray muons;
- `SetMinimumTheta` - Set the minimum zenith angle θ for generated cosmic-ray muons;
- `SetMaximumTheta` - Set the maximum zenith angle θ for generated cosmic-ray muons;
- `SetMinimumPhi` - Set the minimum azimuthal angle ϕ for generated cosmic-ray muons;
- `SetMaximumPhi` - Set the maximum azimuthal angle ϕ for generated cosmic-ray muons.

The example code 6 shows a possible usage of previous methods.

```
#include <math.h> // necessary for the M_PI constant

EcoMug gen;
gen.SetUseSky();
gen.SetSkySize({{10., 10.}});
gen.SetSkyCenterPosition({{0., 0., 20.}});

gen.SetMinimumMomentum(80.);
gen.SetMaximumMomentum(800.);
gen.SetMinimumTheta(0.);
gen.SetMaximumTheta(M_PI/4);
gen.SetMinimumPhi(0.);
gen.SetMaximumPhi(M_PI);
```

Example code 6: Filtering the generation in EcoMug.

The full list of methods of the EcoMug class is available at the following link:
https://dr4kan.github.io/EcoMug/class_eco_mug.html.

5.4. Using a user-defined function for the differential flux

In those cases where the proposed parametrization of J does not provide an accurate description of the differential flux of CR muons, EcoMug gives the possibility to use a custom function for J, as shown in the example code 7.

```
double J(double p, double theta) {
  double A = 0.14*pow(p, -2.7);
  double B = 1. / (1. + 1.1*p*cos(theta)/115.);
  double C = 0.054 / (1. + 1.1*p*cos(theta)/850.);
  return A*(B+C);
}

EcoMug gen;
gen.SetUseSky();
gen.SetSkySize({{x, y}});
gen.SetSkyCenterPosition({0., 0., z});
gen.SetMinimumMomentum(150);
gen.SetDifferentialFlux(&J);

for (auto event = 0; event < nevents; ++event) {
  gen.GenerateFromCustomJ(); // generate from user-defined J
  ... // retrieve and use muon data
  gen.Generate(); // generate from J as in equation 2
  ... // retrieve and use muon data
}
```

Example code 7: Filtering the generation in EcoMug.

In the previous code, the same instance of the class `EcoMug` is used to generate according to a Gaisser-like parametrization [41] and to the default one (Eq. (2)). The use of a custom definition for J requires a function of both momentum and θ to be passed to the generator by means of the method `SetDifferentialFlux`. Afterwards, the user can invoke the generation of a CR muon, according to the specified J, with the method `GenerateFromCustomJ`.

6. Conclusions

It has been presented a new Monte Carlo generator of CR muons, called EcoMug, specifically designed for muon radiography and tomography applications. Based on a parametrization of the experimental data in Fig. 1, EcoMug gives the possibility of generating from different surfaces (plane, cylinder and half-sphere), while keeping the correct angular and momentum distribution of generated tracks. This flexibility, together with the possibility of restricting the angular variables and momentum of muons at generation level, and a fast and optimized code, allows for a very efficient generation of CR muons for those applications requiring high statistics, as typical muon radiography and tomography applications do. For those cases where the proposed parametrization does not provide an accurate description of the differential flux of CR muons, a custom definition of it can be used. The code is freely available at https://github.com/dr4kan/EcoMug under the GPL-3.0 license.

CRediT authorship contribution statement

D. Pagano: Methodology, Formal analysis, Software, Writing - original draft, Writing - review & editing. **G. Bonomi:** Methodology, Formal analysis, Validation. **A. Donzella:** Formal analysis, Validation. **A. Zenoni:** Conceptualization, Methodology, Validation. **G. Zumerle:** Conceptualization, Methodology, Writing - review & editing. **N. Zurlo:** Methodology, Formal analysis, Validation.

Declaration of competing interest

The authors declare that they have no known competing financial interests or personal relationships that could have appeared to influence the work reported in this paper.

Acknowledgments

The authors acknowledge the support from the National Institute of Nuclear Physics (INFN) and from the Universities they belong to. Part of the work was developed within the Mu-Blast project, funded by the Research Fund for Coal and Steel of the European Union (RFSR-CT-2014-00027).

Appendix. Example of integration with GEANT4

EcoMug can be easily integrated with GEANT4, by modifying the (mandatory) user action class derived from `G4VUserPrimaryGeneratorAction`.

The relevant lines of codes to be included in the header file are reported below.

```
#include "EcoMug.h"
...
class PrimaryGeneratorAction :
      public G4VUserPrimaryGeneratorAction {
  public:
  ...
  G4ParticleGun *fParticleGun;
  G4ParticleDefinition *mu_plus, *mu_minus;
  EcoMug fMuonGen;
};
```

The implementation file initializes the class `EcoMug` and interfaces it to `G4ParticleGun`, as shown in the code below.

```
PrimaryGeneratorAction::PrimaryGeneratorAction() :
G4VUserPrimaryGeneratorAction(),
fParticleGun(0), mu_plus(0), mu_minus(0) {
  fMuonGen.SetUseCylinder();
  fMuonGen.SetCylinderRadius(2500*mm);
  fMuonGen.SetCylinderHeight(4170*mm);

  fParticleGun  = new G4ParticleGun(1);
  mu_minus  = G4ParticleTable::GetParticleTable()
              ->FindParticle("mu-");
  mu_plus  = G4ParticleTable::GetParticleTable()
             ->FindParticle("mu+");
}
...
void PrimaryGeneratorAction::GeneratePrimaries(G4Event* ev) {
  fMuonGen.Generate();
  array<double, 3> muon_pos = fMuonGen.GetGenerationPosition();
  double muon_ptot = fMuonGen.GetGenerationMomentum();
  double muon_theta = fMuonGen.GetGenerationTheta();
  double muon_phi = fMuonGen.GetGenerationPhi();
  fParticleGun->SetParticlePosition(G4ThreeVector(
    muon_pos[0]*mm,
    muon_pos[1]*mm,
    muon_pos[2]*mm
  ));

  fParticleGun->SetParticleMomentum(G4ParticleMomentum(
    muon_ptot*sin(muon_theta)*cos(muon_phi)*GeV,
    muon_ptot*sin(muon_theta)*sin(muon_phi)*GeV,
    muon_ptot*cos(muon_theta)*GeV
  ));

  // charge
  if (fMuonGen.GetCharge() < 0) {
    fParticleGun->SetParticleDefinition(mu_minus);
  } else {
    fParticleGun->SetParticleDefinition(mu_plus);
  }
  fParticleGun->GeneratePrimaryVertex(ev);
}
```

References

[1] L.I. Dorman, Cosmic Rays in the Earth's Atmosphere and Underground, Springer Netherlands, 2004, http://dx.doi.org/10.1007/978-1-4020-2113-8.

[2] C. Grupen, Astroparticle Physics, Springer International Publishing, 2020, http://dx.doi.org/10.1007/978-3-030-27339-2.

[3] L. Bonechi, M. Bongi, D. Fedele, M. Grandi, S. Ricciarini, E. Vannuccini, Development of the ADAMO detector: test with cosmic rays at different zenith angles, in: 29th International Cosmic Ray Conference Vol. 9, 2005, pp. 283.

[4] D. Pacini, La radiazione penetrante alla superficie ed in seno alle acque, Il Nuovo Cimento 3 (1) (1912) 93–100, http://dx.doi.org/10.1007/bf02957440.

[5] V.F. Hess, Uber beobachtungen der durchdringenden strahlung bei sieben freiballonfahrten, Phys. Zeits. 13 (1912) 1084–1091.

[6] E. George, Cosmic rays measure overburden of tunnel, Commonw. Eng. 455 (1955).

[7] L.W. Alvarez, J.A. Anderson, F. El Bedwei, J. Burkhard, A. Fakhry, A. Girgis, A. Goneid, F. Hassan, D. Iverson, G. Lynch, et al., Search for hidden chambers in the pyramids, Science 167 (3919) (1970) 832–839.

[8] K.N. Borozdin, G.E. Hogan, C. Morris, W.C. Priedhorsky, A. Saunders, L.J. Schultz, M.E. Teasdale, Radiographic imaging with cosmic-ray muons, Nature 422 (6929) (2003) 277, http://dx.doi.org/10.1038/422277a.

[9] K. Gnanvo, L.V. Grasso III, M. Hohlmann, J.B. Locke, A. Quintero, D. Mitra, Imaging of high-Z material for nuclear contraband detection with a minimal prototype of a muon tomography station based on GEM detectors, Nucl. Instrum. Methods Phys. Res. A 652 (1) (2011) 16–20.

[10] M. Benettoni, G. Bettella, G. Bonomi, G. Calvagno, P. Calvini, P. Checchia, G. Cortelazzo, L. Cossutta, A. Donzella, M. Furlan, F. Gonella, M. Pegoraro, A.R. Garola, P. Ronchese, S. Squarcia, M. Subieta, S. Vanini, G. Viesti, P. Zanuttigh, A. Zenoni, G. Zumerle, Noise reduction in muon tomography for detecting high density objects, J. Instrum. 8 (12) (2013) P12007, http://dx.doi.org/10.1088/1748-0221/8/12/p12007.

[11] D. Poulson, J. Durham, E. Guardincerri, C. Morris, J. Bacon, K. Plaud-Ramos, D. Morley, A. Hecht, Cosmic ray muon computed tomography of spent nuclear fuel in dry storage casks, Nucl. Instrum. Methods Phys. Res. A 842 (2017) 48–53, http://dx.doi.org/10.1016/j.nima.2016.10.040.

[12] G. Bonomi, M. Caccia, A. Donzella, D. Pagano, V. Villa, A. Zenoni, Cosmic ray tracking to monitor the stability of historical buildings: A feasibility study, Meas. Sci. Technol. 30 (4) (2019) 045901, http://dx.doi.org/10.1088/1361-6501/ab00d7.

[13] S. Agostinelli, J. Allison, K. Amako, J. Apostolakis, H. Araujo, P. Arce, M. Asai, D. Axen, S. Banerjee, G. Barrand, F. Behner, L. Bellagamba, J. Boudreau, L. Broglia, A. Brunengo, H. Burkhardt, S. Chauvie, J. Chuma, R. Chytracek, G. Cooperman, G. Cosmo, P. Degtyarenko, A. Dell'Acqua, G. Depaola, D. Dietrich, R. Enami, A. Feliciello, C. Ferguson, H. Fesefeldt, G. Folger, F. Foppiano, A. Forti, S. Garelli, S. Giani, R. Giannitrapani, D. Gibin, J.G. Cadenas, I. González, G.G. Abril, G. Greeniaus, W. Greiner, V. Grichine, A. Grossheim, S. Guatelli, P. Gumplinger, R. Hamatsu, K. Hashimoto, H. Hasui, A. Heikkinen, A. Howard, V. Ivanchenko, A. Johnson, F. Jones, J. Kallenbach, N. Kanaya, M. Kawabata, Y. Kawabata, M. Kawaguti, S. Kelner, P. Kent, A. Kimura, T. Kodama, R. Kokoulin, M. Kossov, H. Kurashige, E. Lamanna, T. Lampén, V. Lara, V. Lefebure, F. Lei, M. Liendl, W. Lockman, F. Longo, S. Magni, M. Maire, E. Medernach, K. Minamimoto, P.M. de Freitas, Y. Morita, K. Murakami, M. Nagamatu, R. Nartallo, P. Nieminen, T. Nishimura, K. Ohtsubo, M. Okamura, S. O'Neale, Y. Oohata, K. Paech, J. Perl, A. Pfeiffer, M. Pia, F. Ranjard, A. Rybin, S. Sadilov, E.D. Salvo, G. Santin, T. Sasaki, N. Savvas, Y. Sawada, S. Scherer, S. Sei, V. Sirotenko, D. Smith, N. Starkov, H. Stoecker, J. Sulkimo, M. Takahata, S. Tanaka, E. Tcherniaev, E.S. Tehrani, M. Tropeano, P. Truscott, H. Uno, L. Urban, P. Urban, M. Verderi, A. Walkden, W. Wander, H. Weber, J. Wellisch, T. Wenaus, D. Williams, D. Wright, T. Yamada, H. Yoshida, D. Zschiesche, Geant4–A simulation toolkit, Nucl. Instrum. Methods Phys. Res. A 506 (3) (2003) 250–303, http://dx.doi.org/10.1016/s0168-9002(03)01368-8.

[14] T. Böhlen, F. Cerutti, M. Chin, A. Fassò, A. Ferrari, P. Ortega, A. Mairani, P. Sala, G. Smirnov, V. Vlachoudis, The FLUKA code: Developments and challenges for high energy and medical applications, Nucl. Data Sheets 120 (2014) 211–214, http://dx.doi.org/10.1016/j.nds.2014.07.049.

[15] D. Heck, T. Pierog, J. Knapp, CORSIKA: An air shower simulation program, Astrophys. Source Code Libr. (2012) ascl–1202.

[16] C. Hagmann, D. Lange, D. Wright, Cosmic-ray shower generator (CRY) for Monte Carlo transport codes, in: 2007 IEEE Nuclear Science Symposium Conference Record, IEEE, 2007, http://dx.doi.org/10.1109/nssmic.2007.4437209.

[17] A. Achterberg, M. Ackermann, J. Adams, J. Ahrens, K. Andeen, D. Atlee, J. Baccus, J. Bahcall, X. Bai, B. Baret, et al., First year performance of the IceCube neutrino telescope, Astropart. Phys. 26 (3) (2006) 155–173.

[18] M.P. van Haarlem, M.W. Wise, A. Gunst, G. Heald, J.P. McKean, J.W. Hessels, A.G. de Bruyn, R. Nijboer, J. Swinbank, R. Fallows, et al., LOFAR: The low-frequency array, Astron. Astrophys. 556 (2013) A2.

[19] J. Aleksić, S. Ansoldi, L.A. Antonelli, P. Antoranz, A. Babic, P. Bangale, M. Barceló, J. Barrio, J.B. González, W. Bednarek, et al., The major upgrade of the MAGIC telescopes, Part II: A performance study using observations of the Crab Nebula, Astropart. Phys. 72 (2016) 76–94.

[20] J.A. Hinton, H. Collaboration, et al., The status of the HESS project, New Astron. Rev. 48 (5–6) (2004) 331–337.

[21] J. Abraham, M. Aglietta, I. Aguirre, M. Albrow, D. Allard, I. Allekotte, P. Allison, J.A. Muniz, M. Do Amaral, M. Ambrosio, et al., Properties and performance of the prototype instrument for the pierre auger observatory, Nucl. Instrum. Methods Phys. Res. A 523 (1–2) (2004) 50–95.

[22] W.R. Nelson, H. Hirayama, D.W. Rogers, EGS4 code system, 1985, URL https://www.osti.gov/biblio/6137659.

[23] K. Kamata, J. Nishimura, The lateral and the angular structure functions of electron showers, Progr. Theoret. Phys. Suppl. 6 (1958) 93–155, http://dx.doi.org/10.1143/PTPS.6.93, arXiv:https://academic.oup.com/ptps/article-pdf/doi/10.1143/PTPS.6.93/5270594/6-93.pdf.

[24] R. Engel, D. Heck, T. Huege, T. Pierog, M. Reininghaus, F. Riehn, R. Ulrich, M. Unger, D. Veberič, Towards a next generation of CORSIKA: A framework for the simulation of particle cascades in astroparticle physics, Comput. Softw. Big Sci. 3 (1) (2018) http://dx.doi.org/10.1007/s41781-018-0013-0.

[25] M. Reininghaus, R. Ulrich, CORSIKA 8 – Towards a modern framework for the simulation of extensive air showers, EPJ Web Conf. 210 (2019) 02011, http://dx.doi.org/10.1051/epjconf/201921002011.

[26] A. Fedynitch, R. Engel, T.K. Gaisser, F. Riehn, T. Stanev, Calculation of conventional and prompt lepton fluxes at very high energy, in: EPJ Web of Conferences, Vol. 99, EDP Sciences, 2015, p. 08001.

[27] L.S. Waters, G.W. McKinney, J.W. Durkee, M.L. Fensin, J.S. Hendricks, M.R. James, R.C. Johns, D.B. Pelowitz, The MCNPX Monte Carlo radiation transport code, in: AIP Conference Proceedings, Vol. 896, (1) American Institute of Physics, 2007, pp. 81–90.

[28] GEMC: GEant4 Monte-Carlo, URL https://gemc.jlab.org/gemc/html/index.html.

[29] A. Dar, Atmospheric neutrinos, astrophysical neutrons, and proton-decay experiments, Phys. Rev. Lett. 51 (3) (1983) 227–230, http://dx.doi.org/10.1103/physrevlett.51.227.

[30] P. Biallass, T. Hebbeker, Parametrization of the cosmic muon flux for the generator CMSCGEN, 2009, arXiv preprint arXiv:0907.5514.

[31] P. Achard, O. Adriani, M. Aguilar-Benitez, M. van den Akker, J. Alcaraz, G. Alemanni, J. Allaby, A. Aloisio, M. Alviggi, H. Anderhub, V. Andreev, F. Anselmo, A. Arefiev, T. Azemoon, T. Aziz, P. Bagnaia, A. Bajo, G. Baksay, L. Baksay, J.

Bähr, S. Baldew, S. Banerjee, S. Banerjee, A. Barczyk, R. Barillère, P. Bartalini, M. Basile, N. Batalova, R. Battiston, A. Bay, F. Becattini, U. Becker, F. Behner, L. Bellucci, R. Berbeco, J. Berdugo, P. Berges, B. Bertucci, B. Betev, M. Biasini, M. Biglietti, A. Biland, J. Blaising, S. Blyth, G. Bobbink, A. Böhm, L. Boldizsar, B. Borgia, S. Bottai, D. Bourilkov, M. Bourquin, S. Braccini, J. Branson, F. Brochu, J. Burger, W. Burger, X. Cai, M. Capell, G.C. Romeo, G. Carlino, A. Cartacci, J. Casaus, F. Cavallari, N. Cavallo, C. Cecchi, M. Cerrada, M. Chamizo, T. Chiarusi, Y. Chang, M. Chemarin, A. Chen, G. Chen, G. Chen, H. Chen, H. Chen, G. Chiefari, L. Cifarelli, F. Cindolo, I. Clare, R. Clare, G. Coignet, N. Colino, S. Costantini, B. de la Cruz, S. Cucciarelli, J. van Dalen, R. de Asmundis, P. Déglon, J. Debreczeni, A. Degré, K. Dehmelt, K. Deiters, D. della Volpe, E. Delmeire, P. Denes, F. DeNotaristefani, A.D. Salvo, M. Diemoz, M. Dierckxsens, L. Ding, C. Dionisi, M. Dittmar, A. Doria, M. Dova, D. Duchesneau, M. Duda, I. Duran, B. Echenard, A. Eline, A.E. Hage, H.E. Mamouni, A. Engler, F. Eppling, P. Extermann, G. Faber, M. Falagan, S. Falciano, A. Favara, J. Fay, O. Fedin, M. Felcini, T. Ferguson, H. Fesefeldt, E. Fiandrini, J. Field, F. Filthaut, W. Fisher, I. Fisk, G. Forconi, K. Freudenreich, C. Furetta, Y. Galaktionov, S. Ganguli, P. Garcia-Abia, M. Gataullin, S. Gentile, S. Giagu, Z. Gong, H. Grabosch, G. Grenier, O. Grimm, H. Groenstege, M. Gruenewald, M. Guida, Y. Guo, S. Gupta, V. Gupta, A. Gurtu, L. Gutay, D. Haas, C. Haller, D. Hatzifotiadou, Y. Hayashi, Z. He, T. Hebbeker, A. Hervé, J. Hirschfelder, H. Hofer, H. Hofer, M. Hohlmann, G. Holzner, S. Hou, A. Huo, Y. Hu, N. Ito, B. Jin, C. Jing, L. Jones, P. de Jong, I. Josa-Mutuberría, V. Kantserov, M. Kaur, S. Kawakami, M. Kienzle-Focacci, J. Kim, J. Kirkby, W. Kittel, A. Klimentov, A. König, E. Kok, A. Korn, M. Kopal, V. Koutsenko, M. Kräber, H. Kuang, R. Kraemer, A. Krüger, J. Kuijpers, A. Kunin, P.L. de Guevara, I. Laktineh, G. Landi, M. Lebeau, A. Lebedev, P. Lebrun, P. Lecomte, P. Lecoq, P.L. Coultre, J.L. Goff, Y. Lei, H. Leich, R. Leiste, M. Levtchenko, P. Levtchenko, C. Li, L. Li, Z. Li, S. Likhoded, C. Lin, W. Lin, F. Linde, L. Lista, Z. Liu, W. Lohmann, E. Longo, Y. Lu, C. Luci, L. Luminari, W. Lustermann, W. Ma, X. Ma, Y. Ma, L. Malgeri, A. Malinin, C.M. na, J. Mans, J. Martin, F. Marzano, K. Mazumdar, R. McNeil, S. Mele, X. Meng, L. Merola, M. Meschini, W. Metzger, A. Mihul, A. van Mil, H. Milcent, G. Mirabelli, J. Mnich, G. Mohanty, B. Monteleoni, G. Muanza, A. Muijs, B. Musicar, M. Musy, S. Nagy, R. Nahnhauer, V. Naumov, S. Natale, M. Napolitano, F. Nessi-Tedaldi, H. Newman, A. Nisati, T. Novak, H. Nowak, R. Ofierzynski, G. Organtini, I. Pal, C. Palomares, P. Paolucci, R. Paramatti, J.-F. Parriaud, G. Passaleva, S. Patricelli, T. Paul, M. Pauluzzi, C. Paus, F. Pauss, M. Pedace, S. Pensotti, D. Perret-Gallix, B. Petersen, D. Piccolo, F. Pierella, M. Pieri, M. Pioppi, P. Piroué, E. Pistolesi, V. Plyaskin, M. Pohl, V. Pojidaev, J. Pothier, D. Prokofiev, J. Quartieri, C. Qing, G. Rahal-Callot, M. Rahaman, P. Raics, N. Raja, R. Ramelli, P. Rancoita, R. Ranieri, A. Raspereza, K. Ravindran, P. Razis, D. Ren, M. Rescigno, S. Reucroft, P. Rewiersma, S. Riemann, K. Riles, B. Roe, A. Rojkov, L. Romero, A. Rosca, C. Rosemann, C. Rosenbleck, S. Rosier-Lees, S. Roth, J. Rubio, G. Ruggiero, H. Rykaczewski, R. Saidi, A. Sakharov, S. Saremi, S. Sarkar, J. Salicio, E. Sanchez, C. Schäfer, V. Schegelsky, V. Schmitt, B. Schoeneich, H. Schopper, D. Schotanus, C. Sciacca, L. Servoli, C. Shen, S. Shevchenko, N. Shivarov, V. Shoutko, E. Shumilov, A. Shvorob, D. Son, C. Souga, P. Spillantini, M. Steuer, D. Stickland, B. Stoyanov, A. Straessner, K. Sudhakar, H. Sulanke, G. Sultanov, L. Sun, S. Sushkov, H. Suter, J. Swain, Z. Szillasi, X. Tang, P. Tarjan, L. Tauscher, L. Taylor, B. Tellili, D. Teyssier, C. Timmermans, S.C. Ting, S. Ting, S. Tonwar, J. Tóth, G. Trowitzsch, C. Tully, K. Tung, J. Ulbricht, M. Unger, E. Valente, H. Verkooijen, R. van de Walle, R. Vasquez, V. Veszpremi, G. Vesztergombi, I. Vetlitsky, D. Vicinanza, G. Viertel, S. Villa, M. Vivargent, S. Vlachos, I. Vodopianov, H. Vogel, H. Vogt, I. Vorobiev, A. Vorobyov, M. Wadhwa, R. Wang, Q. Wang, X. Wang, X. Wang, Z. Wang, M. Weber, R. van Wijk, T. Wijnen, H. Wilkens, S. Wynhoff, L. Xia, Y. Xu, J. Xu, Z. Xu, J. Yamamoto, B. Yang, C. Yang, H. Yang, M.Y. and, X. Yang, Z. Yao, S. Yeh, Z. Yu, A. Zalite, Y. Zalite, C. Zhang, F. Zhang, J. Zhang, S. Zhang, Z. Zhang, J. Zhao, S. Zhou, G. Zhu, R. Zhu, H. Zhuang, Q. Zhu, A. Zichichi, B. Zimmermann, M. Zöller, A. Zwart, Measurement of the atmospheric muon spectrum from 20 to 3000 GeV, Phys. Lett. B 598 (1–2) (2004) 15–32, http://dx.doi.org/10.1016/j.physletb.2004.08.003.

[32] G. Battistoni, A. Margiotta, S. Muraro, M. Sioli, FLUKA as a new high energy cosmic ray generator, Nucl. Instrum. Methods Phys. Res. A 626–627 (2011) S191–S192, http://dx.doi.org/10.1016/j.nima.2010.05.019.

[33] G. Carminati, M. Bazzotti, A. Margiotta, M. Spurio, Atmospheric muons from parametric formulas: A fast generator for neutrino telescopes (MUPAGE), Comput. Phys. Comm. 179 (12) (2008) 915–923, http://dx.doi.org/10.1016/j.cpc.2008.07.014.

[34] G. Battistoni, C. Forti, J. Ranft, Study of the high energy cosmic ray cascades using the dual parton model, Astropart. Phys. 3 (2) (1995) 157–184, http://dx.doi.org/10.1016/0927-6505(94)00039-6.

[35] M. Calicchio, G. Case, C. Demarzo, O. Erriquez, C. Favuzzi, N. Giglietto, E. Nappi, F. Posa, P. Spinelli, F. Baldetti, S. Cecchini, G. Giacomelli, F. Grianti, G. Mandrioli, A. Margiotta, L. Patrizii, G. Sanzani, P. Serra, M. Spurio, S. Ahlen, A. Ciocio, M. Felcini, D. Ficenec, J. Incandela, A. Marin, J. Stone, L. Sulak, W. Worstell, B. Barish, C. Lane, G. Liu, C. Peck, G. Poulard, H. Sletten, S. Cohen, N. Ide, A. Manka, R. Steinberg, G. Battistoni, H. Bilokon, C. Bloise, P. Campana, V. Chiarella, A. Grillo, E. Iarocci, A. Marini, J. Reynoldson, A. Rindi, F. Ronga, L. Satta, M. Spinetti, V. Valente, R. Heinz, S. Mufson, J. Petrakis, P. Monacelli, A. Reale, M. Longo, J. Musser, C. Smith, G. Tarlé, M. Ambrosio, B. Barbarino, F. Grancagnolo, A. Onnembo, V. Palladino, C. Angelini, A. Baldini, C. Bemporad, V. Flaminio, G. Giannini, R. Pazzi, G. Auriemma, M.D. Vincenzi, E. Lamanna, G. Martellotti, O. Palamara, S. Petrera, L. Petrillo, P. Pistilli, G. Rosa, A. Sciubba, M. Severi, P. Green, R. Webb, V. Bisi, P. Guibellino, A.M. Chiesa, L. Ramello, D. Soli, P. Trower, The macro detector at the gran sasso laboratory, Nucl. Instrum. Methods Phys. Res. A 264 (1) (1988) 18–23, http://dx.doi.org/10.1016/0168-9002(88)91095-9.

[36] L. Bonechi, Misure di Raggi Cosmici a Terra con l'Esperimento ADAMO (Ph.D. thesis), Università degli Studi di Firenze, Dipartimento di Fisica, 2004.

[37] G. Casella, C.P. Robert, M.T. Wells, Generalized accept-reject sampling schemes, in: Institute of Mathematical Statistics Lecture Notes - Monograph Series, Institute of Mathematical Statistics, 2004, pp. 342–347, http://dx.doi.org/10.1214/lnms/1196285403.

[38] X. Hu, L.S. Ökvist, E. Åström, F. Forsberg, P. Checchia, G. Bonomi, I. Calliari, P. Calvini, A. Donzella, E. Faraci, et al., Exploring the capability of muon scattering tomography for imaging the components in the blast furnace, ISIJ Int. (2017) ISIJINT–2017.

[39] N. Zurlo, C. Amsler, M. Antonello, A. Belov, G. Bonomi, R. Brusa, M. Caccia, A. Camper, R. Caravita, F. Castelli, G. Cerchiari, D. Comparat, G. Consolati, A. Demetrio, L.D. Noto, M. Doser, M. Fanì, R. Ferragut, S. Gerber, M. Giammarchi, A. Gligorova, L. Gloggler, F. Guatieri, S. Haider, A. Hinterberger, A. Kellerbauer, O. Khalidova, D. Krasnický, V. Lagomarsino, C. Malbrunot, S. Mariazzi, V. Matveev, S. Müller, G. Nebbia, P. Nedelec, M. Oberthaler, E. Oswald, D. Pagano, L. Penasa, V. Petracek, F. Prelz, M. Prevedelli, B. Rienaecker, O. Røhne, A. Rotondi, H. Sandaker, R. Santoro, G. Testera, I. Tietje, V. Toso, T. Wolz, P. Yzombard, C. Zimmer, Calibration and equalisation of plastic scintillator detectors for antiproton annihilation identification over positron/positronium background, Acta Phys. Polon. B 51 (1) (2020) 213, http://dx.doi.org/10.5506/aphyspolb.51.213.

[40] V.S. Blackman D., xoshiro / xoroshiro generators and the PRNG shootout, URL https://prng.di.unimi.it/.

[41] T.K. Gaisser, R. Engel, E. Resconi, Cosmic Rays and Particle Physics, Cambridge University Press, 2016.